ELSEVIER

Journal of Nuclear Materials 312 (2003) 81–96

journal of nuclear materials

www.elsevier.com/locate/jnucmat

Modelling the activity of ^{129}I in the primary coolant of a CANDU reactor

Brent J. Lewis [a,*], Aamir Husain [b]

[a] *Department of Chemistry and Chemical Engineering, Royal Military College of Canada, P.O. Box 1700, Kingston, Ont., Canada K7K 7B4*

[b] *Kinectrics Inc., 800 Kipling Avenue, Toronto, Ont., Canada M8Z 6C4*

Received 21 June 2002; accepted 21 October 2002

Abstract

A mathematical treatment has been developed to describe the activity levels of ^{129}I as a function of time in the primary heat transport system during constant power operation and for a reactor shutdown situation. The model accounts for a release of fission-product iodine from defective fuel rods and tramp uranium contamination on in-core surfaces. The physical transport constants of the model are derived from a coolant activity analysis of the short-lived radioiodine species. An estimate of 3×10^{-9} has been determined for the coolant activity ratio of $^{129}I/^{131}I$ in a CANDU Nuclear Generating Station (NGS), which is in reasonable agreement with that observed in the primary coolant and for plant test resin columns from pressurized and boiling water reactor plants. The model has been further applied to a CANDU NGS, by fitting it to the observed short-lived iodine and long-lived cesium data, to yield a coolant activity ratio of $\sim 2 \times 10^{-8}$ for $^{129}I/^{137}Cs$. This ratio can be used to estimate the levels of ^{129}I in reactor waste based on a measurement of the activity of ^{137}Cs.

1. Introduction

Scaling factors are generally employed to estimate the concentrations of difficult-to-measure (DTM) radionuclides. They relate the activity of DTM radionuclides to the activity of easy-to-measure (ETM) gamma-emitting marker radionuclides such as ^{60}Co and ^{137}Cs. Scaling factors for several radionuclides of potential interest to Ontario Power Generation (OPG), namely, ^{238}Pu, ^{239}Pu, ^{240}Pu, ^{241}Pu, ^{241}Am, ^{242}Cm, ^{244}Cm, ^{55}Fe, ^{63}Ni, ^{14}C and ^{90}Sr have been under development since 1999 [1].

Due to the much lower concentrations of many of the remaining DTM radionuclides of interest, such as ^{129}I and ^{99}Tc, their experimental scaling factor development poses a major challenge and theoretical treatments have been proposed for their estimation [2–5]. Such treatments implicitly assume that the scaling factor for radioactive waste can be estimated from coolant activities; departure from this assumption can be empirically accounted for using an experimentally derived correction factor. The PROFIP code, for instance, has been developed to estimate coolant activity concentrations of fission products and actinides in pressurized water reactors (PWRs) [3]. Similarly, the 3R-STAT code focuses on an estimation of ^{129}I and ^{99}Tc coolant activities using measured activities of ^{60}Co, ^{137}Cs and short-lived radioiodine species [5].

Long and short-lived fission products are released into the primary heat transport system (PHTS) as a result of defective fuel operation and from tramp uranium contamination on in-core surfaces [6]. CANDU nuclear generating stations (NGS) routinely sample the short-lived radioiodine and noble gas species in the PHTS by employing online monitoring and/or grab sample

* Corresponding author. Tel.: +1-613 541 6611; fax: +1-613 542 9489.

E-mail address: lewis-b@rmc.ca (B.J. Lewis).

0022-3115/03/$ - see front matter
PII: S0022-3115(02)01588-X

analysis. Thus, these coolant activity measurements can serve as a means for estimating the coolant activity of long-lived α and β emitting nuclides, including that of ^{129}I via a scaling factor analysis. The current work presents the development of a method for predicting the coolant activity of the long-lived ^{129}I, and its scaling factor relative to that of ^{137}Cs, based on the measured activities of the short-lived iodines, namely, ^{131}I, ^{132}I, ^{133}I, ^{134}I and ^{135}I. This prediction is based on a model that considers the physical mechanisms of release for the iodine species from defective CANDU fuel rods and uranium contamination on in-core surfaces. Thus, the application for this work is for the assessment of the ^{129}I activity in waste packages based on ^{137}Cs gamma emission.

2. Model development

With the occurrence of defective fuel, volatile fission products that are released from the solid fuel matrix into the fuel-to-clad gap can migrate along the gap to the defect site where they may be released into the PHTS. Fission products are also generated by the fission of tramp uranium on in-core piping and fuel bundle surfaces. For instance, in a defective rod, grain boundary oxidation of the fuel matrix can occur under the defect site, which in turn can result in particulate fuel loss into the PHTS [6,7]. In addition, uranium contamination may also be present on fuel bundle surfaces as a result of the fuel manufacturing process. These surface fission mechanisms will therefore result in a further burden of fission products into the PHTS. Some of the fission products released from either the defective fuel or tramp uranium will be dissolved in the reactor coolant or remain as particulate fission products. Such material can be removed from the PHTS with the operation of coolant cleanup systems. For example, the radioiodine species will accumulate on the resins of the ion-exchange columns during coolant cleanup operations.

Models are presented in the following sections, describing the release behaviour of volatile fission products from defective fuel rods (Section 2.1) and from uranium contamination on in-core surfaces (Section 2.2).

2.1. Fission product release from defective fuel elements

Fission products can be released from the uranium dioxide fuel into the free void space (fuel-to-clad gap) within the fuel element via solid-state lattice diffusion. Athermal release can also occur by surface fission processes [8]. For instance, release from external surfaces can occur by direct recoil when a fission fragment, with a kinetic energy of ~80 MeV, is produced within a surface layer with a thickness less than or equal to its range in the solid. Another temperature-independent process of release is by knockout, when either a primary fragment or energetic particle created in a collision cascade interacts elastically with a fission product atom. Models detailing these transport mechanisms from the solid fuel into the fuel-to-clad gap are detailed below.

2.1.1. Diffusion

The mass balance equations for describing the concentration distribution $C(r,t)$ (atom m^{-3}) in an 'idealized' fuel grain sphere of radius a, which results at time t from a production by fission β (atom m^{-3} s^{-1}) with losses by diffusion and radioactive decay, is [9,10]:

$$\frac{\partial C}{\partial t} = \frac{D}{r^2}\frac{\partial}{\partial r}\left(r^2\frac{\partial C}{\partial r}\right) - \lambda C + \beta, \tag{1}$$

where λ is the radioactive decay constant (s^{-1}) and D is the diffusion coefficient for a given fission product species in the fuel matrix (m^2 s^{-1}). Eq. (1) is subject to an initial condition of a zero concentration throughout the sphere, i.e.,

$$C(r,0) = 0, \quad 0 < r < a, \ \ t = 0. \tag{2a}$$

For the boundary conditions, the fission product concentration must be finite at the centre of the sphere with a zero concentration at its surface such that:

$$C(0,t) = \text{finite}, \quad r = 0, \ \ t > 0 \tag{2b}$$

and

$$C(a,t) = 0, \quad r = a, \ \ t > 0. \tag{2c}$$

From the Fick's law of diffusion, the release rate from the fuel grain per unit volume, R_f (atom m^{-3} s^{-1}), is given by:

$$R_f = \frac{4\pi a^2}{(4\pi a^3/3)}\left(-D\frac{\partial C}{\partial r}\bigg|_{r=a}\right) = -\frac{3D}{a}\frac{\partial C}{\partial r}\bigg|_{r=a}, \tag{3}$$

which can be directly evaluated with a knowledge of the concentration profile $C(r)$. The release rate in Eq. (3) is evaluated as [11,12]:

$$R_f(t) = 3\beta\left[\frac{1}{\sqrt{\mu}}\coth\sqrt{\mu} - \frac{1}{\mu}\right] - 6\beta e^{-\mu\tau}\sum_{n=1}^{\infty}\left[\frac{e^{-n^2\pi^2\tau}}{n^2\pi^2+\mu}\right]$$
$$\Rightarrow \left(\frac{R}{B}\right)_{\text{dif}} = 3\left[\frac{1}{\sqrt{\mu}}\coth\sqrt{\mu} - \frac{1}{\mu}\right] - 6e^{-\mu\tau}\sum_{n=1}^{\infty}\left[\frac{e^{-n^2\pi^2\tau}}{n^2\pi^2+\mu}\right] \tag{4a}$$

or equivalently written as [11]:

$$R_f = 3\beta\left[\frac{1}{\sqrt{\mu}}\text{erf}(\sqrt{\mu\tau}) - \frac{(1-e^{-\mu\tau})}{\mu}\right] + E \tag{4b}$$

and

$$E = \frac{3\beta}{\sqrt{\mu}} \sum_{n=1}^{\infty} e^{-2n\sqrt{\mu}} \operatorname{erfc}\left(\frac{n}{\sqrt{\tau}} - \sqrt{\mu\tau}\right) - e^{2n\sqrt{\mu}} \operatorname{erfc}\left(\frac{n}{\sqrt{\tau}} + \sqrt{\mu\tau}\right),$$

where $\mu = \lambda/D'$, $\tau = D't$ and $D' = D/a^2$. Eq. (4b) permits a more accurate solution for $\tau \leqslant 0.1$, where E can be neglected. On defining $R = R_f V$ (atom s^{-1}) and $B = \beta V = F\dot{V}y$ (atom s^{-1}) (in which F is the fission rate density (fission $m^{-3}\,s^{-1}$), y is the cumulative fission yield (atom fission^{-1}) and V is the volume of fuel), a conventional release-to-birth rate (R/B) ratio for diffusion follows in the second relation of Eq. (4a). As determined in Section 3.1, the effect of fuel stoichiometry on the diffusivity can be incorporated into the model by using an empirical diffusion coefficient that is evaluated from measured coolant activity data (which results from fission product release from defective fuel rods).

The short-lived radioactive species generally reach a steady-state condition within about three half-lives. In this case, Eq. (4a) reduces to the well known steady-state result for 'Booth diffusion' for the radioactive species of interest [13]:

$$\left(\frac{R}{B}\right)_{\text{dif}} = 3\left[\frac{1}{\sqrt{\mu}} \coth\sqrt{\mu} - \frac{1}{\mu}\right] \approx \frac{3}{\sqrt{\mu}} = 3\sqrt{\frac{D'}{\lambda}}. \tag{5}$$

Similarly, for the stable isotopes, where $\lambda = 0$ (or $\mu \to 0$):

$$\left(\frac{R}{B}\right)_{\text{dif}} = \left[1 - \frac{6}{\pi^2} \sum_{n=1}^{\infty} \frac{e^{-n^2\pi^2\tau}}{n^2}\right] \tag{6a}$$

and the short-time approximation for Eq. (6a) is:

$$\left(\frac{R}{B}\right)_{\text{dif}} = \left[6\sqrt{\frac{\tau}{\pi}} - 3\tau\right]. \tag{6b}$$

2.1.2. Recoil

In the recoil process, primary fission fragments born within a distance of their maximum range from the fuel surface will be instantaneously released into the fuel-to-clad gap of a fuel element. However, these particles typically have sufficient energy to embed themselves in the adjacent fuel cladding. The release of fission products by this process therefore depends on a release efficiency, ε, for these particles to stop in the gas-filled gap. Thus, the release-to-birth rate (R/B) is given by [8]:

$$\left(\frac{R}{B}\right)_{\text{rec}} = \varepsilon\left(\frac{S_g}{V}\right)\mu_f, \tag{7}$$

where S_g/V is the geometrical surface area to volume of the solid and μ_f is the fission fragment range in the solid UO_2. For instance, the primary iodine fragment, which carries ~67 MeV of the available fission energy, has a range of 8.2 mg cm^{-2} so that for a solid UO_2 fuel density of 10.7 g cm^{-3}, $\mu_f = 7.7$ μm [8]. Here the release efficiency is defined as the fraction of those fragments, born within a distance μ_f of a planar surface, which stop in the gas-filled interspace, such that [8]:

$$\varepsilon = \frac{t}{2\mu_g}. \tag{8}$$

In Eq. (8), t is the thickness of the radial gap and μ_g is the maximum range of the fission fragment in the gap. With a defective fuel element under normal operating conditions, the gap is filled with steam at a typical temperature of ~670 K and pressure of 10 MPa (i.e., steam density of 3.79×10^{-2} g cm^{-3}). Hence, given that the iodine fragment has a range of 1.95 mg cm^{-2} in H_2O [8], $\mu_g = 0.51$ mm. The range of the fission fragment does not significantly change if the primary coolant is D_2O as for a CANDU reactor [14]. For a typical gap thickness of $t = 20$ μm, the efficiency for a fission fragment to stop in the gap is therefore evaluated as ~2%. This quantity is significantly smaller than for the case of a planar surface without the presence of any encapsulating surface where $\varepsilon = 1/4 = 25\%$ [8,15]. Due to this small efficiency, recoil is not an important process of release in operating fuel rods, except for the very short-lived fission products.

2.1.3. Knockout

When a fission fragment strikes a stationary atom of the lattice, a primary knock-on may be created. In most circumstances, the primary atom is likely to be a uranium or oxygen atom of the fuel, although occasionally a stationary fission product atom may be dislodged. Similarly, the primary knock-on can also transfer kinetic energy to other atoms of the lattice by elastic collision, creating secondary and in turn, higher-order knock-ons. To a first approximation, the fission products can be considered to be knocked on in the same manner as the uranium atoms of the lattice [15]. For the knock-on of uranium atoms in the UO_2 lattice, it is the higher-order knock-ons which dominate the release since a much larger number of them are created per fission fragment despite their smaller range.

From Fig. 1, given that P_i is the rate of generation of particles of species i per unit volume at the distance x from the solid fuel surface, the rate of particle production in a thin layer of unit area δx cm thick is $P_i\,\delta x$. Of these particles, δI $(= P_i\,\delta x \sin\theta\,\delta\theta\delta\phi/4\pi)$ are moving in a solid angle increment $\delta\Omega$. The total current I_t (particles cm^{-2} s^{-1}) for particle ejection from the solid surface is therefore derived as [8,15]:

$$I_t = \frac{P_i}{4\pi} \int_{x=0}^{\mu} \int_{\phi=0}^{2\pi} \int_{\theta=0}^{\cos^{-1}(x/\mu_p)} \sin\theta\,d\theta\,d\phi\,dx = \frac{P_i\mu_p}{4}, \tag{9}$$

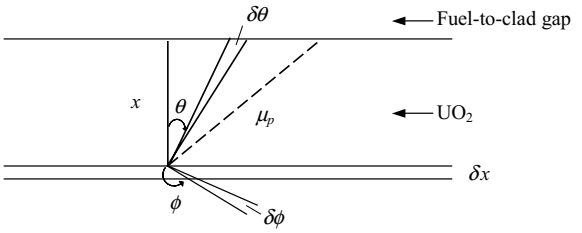

Fig. 1. Schematic for calculating the surface current release from the solid fuel for either a recoil or knockout process for a particle p with a range μ_p.

where μ_p is the maximum range of the particle p (= fission fragment (f) or knock-on (ko)) leaving the solid. Here only those particles within the angle $\theta = \cos^{-1}(x/\mu_p)$ to the normal are capable of escape. For a uniform fission density in the solid, the source term for the fission recoil process is [8,15]

$$P_i^{\mathrm{rec}} = F y_i^{\mathrm{d}}, \tag{10}$$

where F is the fission rate per unit volume and y_i^{d} is the direct fission yield of species i. Moreover, on the premise that the ejection of the uranium atoms result from a cascade of higher-order knock-ons, the knock-on generation rate for a given fission product i is given by [8,15]:

$$P_i^{\mathrm{ko}} = P_{\mathrm{U}}^{\mathrm{ko}} \frac{C_i}{N_{\mathrm{U}}} = (2 n_{\mathrm{U}}^{\mathrm{ko}} F) \frac{C_i}{N_{\mathrm{U}}}, \tag{11}$$

where $n_{\mathrm{U}}^{\mathrm{ko}}$ is the number of uranium knock-ons created by a single fission fragment $\sim 2 \times 10^4$ atoms, C_i is the fission product concentration for species i, and $N_{\mathrm{U}} (= \rho_{\mathrm{UO_2}} N_{\mathrm{A}} / M_{\mathrm{UO_2}})$ is the number density of uranium atoms in the solid (where $\rho_{\mathrm{UO_2}}$ and $M_{\mathrm{UO_2}}$ are the density and molecular weight of the UO_2, respectively, and N_{A} is Avogadro's number) [8,15]. The factor of 2 in Eq. (11) arises since two fragments are created per fission event. Using Eqs. (9) and (10), and summing over all fission products for a total fission yield of 2, the total recoil surface current from fission fragments is:

$$I_{ff}^{\mathrm{rec}} = \sum_{\text{all fission products}} \frac{1}{4} P_i^{\mathrm{rec}} \mu_{\mathrm{f}} = \frac{1}{4} (2F) \mu_{\mathrm{f}}. \tag{12}$$

Similarly, the total surface current for the knockout of uranium atoms is:

$$I_{\mathrm{U}}^{\mathrm{ko}} = \frac{1}{4} P_{\mathrm{U}}^{\mathrm{ko}} \mu_{\mathrm{U}}^{\mathrm{ko}} = \frac{1}{4} (2 n_{\mathrm{U}}^{\mathrm{ko}} F) \mu_{\mathrm{U}}^{\mathrm{ko}}, \tag{13}$$

where $\mu_{\mathrm{U}}^{\mathrm{ko}}$ is the range of the higher-order uranium knock-on in the UO_2 (~ 50 Å) [15]. Thus, the number of uranium atoms emitted per escaping fission fragment α_{U} can be calculated by simply taking the ratio of the corresponding surface currents in Eqs. (12) and (13):

$$\alpha_{\mathrm{U}} = \frac{I_{\mathrm{U}}^{\mathrm{ko}}}{I_{ff}^{\mathrm{rec}}} = n_{\mathrm{U}}^{\mathrm{ko}} \left(\frac{\mu_{\mathrm{U}}^{\mathrm{ko}}}{\mu_{\mathrm{f}}} \right) \approx 9. \tag{14}$$

In fact, the theoretical value for α_{U} in Eq. (14) is in good agreement with a value of ~ 5 as measured for sintered UO_2 [16,17], which provides support for the current theoretical treatment.

The knockout current of species i follows similarly from Eqs. (11) and (13) as:

$$I_i^{\mathrm{ko}} = I_{\mathrm{U}}^{\mathrm{ko}} \left(\frac{C_i}{N_{\mathrm{U}}} \right) = \frac{1}{4} (2 n_{\mathrm{U}}^{\mathrm{ko}} F) \mu_{\mathrm{U}}^{\mathrm{ko}} \left(\frac{C_i}{N_{\mathrm{U}}} \right). \tag{15}$$

Eq. (15) is identical in form to that proposed for the PROFIP Code, where a volume of fuel ejected per fission fragment is equivalently defined as $v = n_{\mathrm{U}}^{\mathrm{ko}} / N_{\mathrm{U}}$ [3]. However, a recoil zone thickness of μ_{f} (as defined by ρ in the PROFIP code) is incorrectly proposed in the PROFIP model in place of the knockout zone thickness of $\mu_{\mathrm{U}}^{\mathrm{ko}}$ as per Eq. (15).

The corresponding release-to-birth rate ratio for knockout results from Eqs. (14) and (15):

$$\left(\frac{R}{B} \right)_{\mathrm{ko}} = \left(\frac{S_t}{V} \right) \frac{\alpha_{\mathrm{U}} \mu_{\mathrm{f}}}{2 y_i} \left(\frac{C_i}{N_{\mathrm{U}}} \right) \tag{16}$$

using the definition of the birth rate, $B = y_i F V$. Here S_t/V is the ratio of the total surface area to volume of the solid. The total surface area of the solid arises since the initial kinetic energy of the higher-order knock-on is sufficiently low (~ 200 eV) that these particles can be easily stopped within small cracks of the fuel so that a release can also occur from these cracked surfaces.

The concentration of fission products C_i near the surface of the solid fuel (i.e., within a knockout zone of ~ 50 Å) can be evaluated from the mass balance equation for a source from the fission process and loss by radioactive decay:

$$\frac{\mathrm{d}C_i}{\mathrm{d}t} = \frac{1}{2} y_i F - \lambda_i C_i. \tag{17}$$

The factor of $1/2$ in Eq. (17) arises due to symmetry arguments where the concentration near the surface is only receiving one half of the fission product generation. The solution of Eq. (17), assuming that $C_i = 0$ at $t = 0$, is:

$$C_i(t) = \frac{F y_i}{2 \lambda_i} (1 - \mathrm{e}^{-\lambda_i t}). \tag{18}$$

Thus, substituting Eq. (18) into (16) gives

$$\left(\frac{R}{B} \right)_{\mathrm{ko}} = \frac{S_t}{V} \left(\frac{\alpha_{\mathrm{U}} \mu_{\mathrm{f}}}{4 \lambda_i N_{\mathrm{U}}} \right) F [1 - \mathrm{e}^{-\lambda_i t}]. \tag{19}$$

In fact, in the steady state, where $t \to \infty$, Eq. (19) reduces to

$$\left(\frac{R}{B}\right)_{\mathrm{ko}} = \frac{S_t}{V}\left(\frac{\alpha_{\mathrm{U}}\mu_{\mathrm{f}}}{4\lambda_i N_{\mathrm{U}}}\right)F. \tag{20}$$

This expression is identical to that derived in Ref. [8], based on a more complicated mass-balance treatment. As depicted in Eq. (20), the release rate is inversely dependent on the decay constant λ_i but proportional to the square of the fission density F, as first suggested by Carroll and Sisman [18]. For the short-lived species, as follows from Eqs. (5) and (20), knockout is an inefficient process for release as compared to diffusion for typical CANDU fuel power ratings [8]. Moreover, the ratio of Eq. (20) to (7) is typically much less than unity so that knockout is also less important compared to that of recoil.

Finally, for the stable species, on letting λ_i approach zero in the limit, Eq. (19) becomes

$$\left(\frac{R}{B}\right)_{\mathrm{ko}} = \frac{S_t}{V}\left(\frac{\alpha_{\mathrm{U}}\mu_{\mathrm{f}}}{4N_{\mathrm{U}}}\right)Ft. \tag{21}$$

Once again, Eq. (21) is negligible compared to Eq. (6) for typical fuel rod burnups and power ratings [8].

Hence, the treatment proposed by Vance [4,5] to account for the temperature-independent release contributions from both recoil and knockout into the fuel-to-clad gap of defective fuel rods is not required for a physical scaling model. Moreover, the knockout model used by Vance was based on the PROFIP code treatment [3], which used a layer thickness of ~10 μm (corresponding to a recoil thickness layer) in place of a much smaller knockout layer distance of ~50 Å as previously discussed. The use of the PROFIP model would therefore overemphasize the importance of the knockout process.

2.1.4. Mass balance in the fuel-to-clad gap

As previously demonstrated, recoil and knockout are not important release processes into the fuel-to-clad gap as compared to diffusion in operating defective fuel rods. Volatile fission products that are released into the gap will migrate towards the defect site where they may be eventually released into the reactor coolant. This transport can be treated as a first-order rate process, as characterized by a gap escape rate coefficient v [10]. A mass balance equation can be written for the fission product inventory (N_{g}) in the fuel-to-clad gap, where on accounting for a source due to a diffusional release from the fuel matrix (R_{dif}) (i.e., as follows from Eq. (4)) and losses due to radioactive decay and release from the defective rod:

$$\frac{\mathrm{d}N_{\mathrm{g}}}{\mathrm{d}t} = R_{\mathrm{dif}} - (\lambda + v)N_{\mathrm{g}}. \tag{22}$$

The solution of Eq. (22) for the radioactive species is:

$$N_{\mathrm{g}}(t) = \frac{3B}{(\lambda+v)}\left[\frac{1}{\sqrt{\mu}}\coth\sqrt{\mu} - \frac{1}{\mu}\right](1-\mathrm{e}^{-(\mu+\psi)\tau}) - \frac{6B\mathrm{e}^{-\mu\tau}}{D'}\sum_{n=1}^{\infty}\frac{\mathrm{e}^{-\psi\tau}-\mathrm{e}^{-n^2\pi^2\tau}}{(n^2\pi^2-\psi)(n^2\pi^2+\mu)}, \tag{23}$$

where $\psi = v/D'$.

The subsequent rate of fission product release from the gap and into the coolant can be evaluated from:

$$R_c(t) = vN_{\mathrm{g}}(t) \tag{24}$$

so that

$$R_c(t) = \frac{3Bv}{(\lambda+v)}\left[\frac{1}{\sqrt{\mu}}\coth\sqrt{\mu} - \frac{1}{\mu}\right](1-\mathrm{e}^{-(\mu+\psi)\tau}) - 6B\psi\mathrm{e}^{-\mu\tau}\sum_{n=1}^{\infty}\frac{\mathrm{e}^{-\psi\tau}-\mathrm{e}^{-n^2\pi^2\tau}}{(n^2\pi^2-\psi)(n^2\pi^2+\mu)}. \tag{25}$$

Moreover, since the short-lived radionuclides typically reach an equilibrium situation quite rapidly, Eq. (25) yields the well known release-to-birth rate ratio for fission product release into the coolant during steady-state conditions [3,6,7,10,19–21]:

$$\frac{R_c}{B} = 3\left(\frac{v}{\lambda+v}\right)\left[\frac{1}{\sqrt{\mu}}\coth\sqrt{\mu} - \frac{1}{\mu}\right] \approx 3\left(\frac{v}{\lambda+v}\right)\sqrt{\frac{D'}{\lambda}}. \tag{26}$$

Similarly, for the stable isotopes, using Eq. (22) with $\lambda = 0$, gives:

$$N_{\mathrm{g}}(t) = \frac{B}{D'}\left[\frac{(1-\mathrm{e}^{-\psi\tau})}{\psi} - 6\sum_{n=1}^{\infty}\frac{\mathrm{e}^{-\psi\tau}-\mathrm{e}^{-n^2\pi^2\tau}}{n^2\pi^2(n^2\pi^2-\psi)}\right] \tag{27}$$

and the release rate into the coolant is:

$$R_c(t) = B\left[(1-\mathrm{e}^{-\psi\tau}) - 6\psi\sum_{n=1}^{\infty}\frac{\mathrm{e}^{-\psi\tau}-\mathrm{e}^{-n^2\pi^2\tau}}{n^2\pi^2(n^2\pi^2-\psi)}\right]. \tag{28}$$

In summary, Eqs. (25) or (28) account for the release of radioactive or stable fission products from the defective fuel rod into the primary coolant. In addition to this source, there is also a release into the coolant from uranium debris deposited on in-core surfaces (Section 2.2).

2.2. Fission product release from tramp uranium

As discussed, uranium contamination resulting from a previous fuel loss from defective fuel rods or from the fuel manufacturing process can lead to additional activity in the PHTS when this contamination is deposited on in-core surfaces. Generally, such contamination is in the form of fine fuel debris. For instance, with defective

rods, grain boundary oxidation results when the coolant contacts the solid fuel pellet under the defect site, leading to a washout of the individual fuel grains [6]. The possibility for dissolution of UO_2 near the defect site is expected to be extremely small in an alkaline coolant (pH $\sim$ 10) at a coolant temperature of $\sim$300 °C [22]. As such, the fuel debris will be typically in the form of small particles that are roughly spherical, with a diameter comparable to that of the grain radius of $\sim$10 μm [6]. As a result of a small particle size, the temperature generated by fission heating is generally too low for diffusion to be an important transport process. As such, temperature-independent processes, such as recoil or knockout, now become the dominant release mechanisms.

For the geometry of a spherical fuel particle with a diameter d_p, and with no other solid surfaces in its vicinity, the release efficiency ε can be described as [8,23]:

$$\varepsilon = \frac{1}{2}\left\{\frac{d}{3\alpha^3} + \frac{1}{2}\left(1 - \frac{1}{\alpha^2}\right)\right\}, \tag{29}$$

where $\alpha = \max(1, d)$ and $d = d_p/\mu_p$. Thus, in the case of a recoil process, the range of the fission fragment (where $\mu_p = \mu_f$) is comparable to the diameter of the fuel particle so that $\alpha = 1$, and Eq. (29) becomes:

$$\varepsilon = \frac{d}{6} = \frac{d_p}{6\mu_f}. \tag{30}$$

Hence, given a surface-to-volume ratio for the spherical particle of $(S_g/V) = 6/d_p$, the release-to-birth ratio in Eq. (7) reduces to:

$$\left(\frac{R}{B}\right)_{rec} = 1. \tag{31}$$

This result is to be expected since any fission fragment generated in the small fuel particle has a sufficiently long range so that it is instantaneously released into the coolant.

If the fuel particle is deposited on a piping surface, the release into the coolant will be one half of that for a particle suspended in the coolant from symmetry arguments since the fission fragment has sufficient kinetic energy to embed itself into the underlying piping surface such that:

$$\left(\frac{R}{B}\right)_{rec} = \frac{1}{2}. \tag{32}$$

In the case of knockout, the range of the knockout particle (i.e., $\mu_U^{ko} \sim 50$ Å) is very small compared to the size of the fuel particle ($d_p \sim 10$ μm) so that $\alpha = d = d_p/\mu_p \gg 1$ in Eq. (29) and the release efficiency is therefore evaluated as:

$$\varepsilon = \frac{1}{2}\left\{\frac{1}{3d^2} + \frac{1}{2}\left(1 - \frac{1}{d^2}\right)\right\} \approx \frac{1}{4}. \tag{33}$$

This result is to be expected as it is also the limiting form for the planar surface calculation of Fig. 1 and Eq. (13). Hence, Eq. (16) further applies to this situation, and on assuming that the total surface area equals roughly three times the geometric one [24], and noting that $d_p \approx \mu_f$, the R/B ratio for knockout is:

$$\left(\frac{R}{B}\right)_{ko} \approx \frac{9\alpha_U}{y_i}\left(\frac{C_i}{N_U}\right). \tag{34}$$

In the case of fuel loss from defective fuel rods, the fission product concentration C_i in Eq. (34) will depend on that previously generated in the fuel rod, as well as that generated later in the fuel debris on the piping surfaces. However, in the latter situation for fuel particles deposited on a surface, very few of the isotropically released fission fragments will actually be directed towards adjacent fuel particles (as a result of the limited solid angle), where they could possibly come to rest. Instead, the majority of fragments will be released directly and instantaneously into the coolant during the primary recoil event. In fact, for the original uranium contamination found on outer surfaces of the fuel bundle, the latter argument specifically applies where $C_i \sim 0$ in Eq. (34). Moreover, for typical fuel burnups it can also be shown that Eq. (34) is much less than 1/2 (i.e., the ratio in Eq. (32)), so that recoil predominates as the low-temperature release process. (Recall that knockout is also negligible for fuel with dimensions much greater than the recoil range.) For instance, experimental ratios of release rates of $^{88}Kr/^{138}Xe$ were between 0.4 and 0.7 in a pressurized-water loop containing fuel debris on the piping surface [25]. This range is in excellent agreement with the theory of recoil, where by Eq. (32):

$$R_{Kr-88}/R_{Xe-138} = y_{Kr-88}/y_{Xe-138} = 0.55.$$

(The cumulative fission yield has been used above to account for the decay of precursor products, which are also emitted into the recirculating coolant.) Moreover, Eq. (32) has been successfully used to distinguish fission product release from fuel failures from that of uranium contamination in fuel-failure monitoring analyses [6–8,20,21].

3. Model application: scaling factor analysis

The fission product release models developed for defective fuel and tramp uranium contamination in Section 2, can be used to provide a scaling factor for the estimation of the coolant activity of the long-lived isotope, ^{129}I. In particular, by fitting the release model to the measured coolant activity data for the short-lived iodine isotopes (Section 3.1), the fitted model parameters can then be used for the prediction of ^{129}I (Section 3.2).

3.1. Short-lived iodine analysis (steady-state)

The fission product inventory in the reactor coolant (N_c) can be determined by a mass balance of the source release from both defective fuel rod(s) and uranium contamination and losses due to radioactive decay and coolant purification:

$$\frac{dN_c}{dt} = R_c^t - (\lambda + \beta_p)N_c. \tag{35}$$

Here β_p is a coolant purification rate constant (s^{-1}) ($= f_p\varepsilon_p/M$, where f_p is the cleanup system flow rate (kg/s), ε_p is the cleanup system efficiency and M is the mass of water in the PHTS (kg)). The total release rate into the coolant,

$$R_c^t(t) = R_c(t) + R_{rec}, \tag{36}$$

is derived from a summation of that from defective fuel rod(s), $R_c(t)$ in Eqs. (25) or (26), and uranium contamination, R_{rec} in Eq. (32).

As mentioned, the short-lived species generally reach an equilibrium activity quite rapidly. Thus, for the steady-state situation, Eqs. (26), (32) and (36) yield the combined result

$$\left(\frac{R}{y}\right)_c = \left(\frac{v}{\lambda + v}\right)\frac{A}{\sqrt{\lambda}}H + c, \tag{37}$$

where $A = x(3\sqrt{D'}F_f)$ and $c = (1/2)F_t$. Here x is the number of defective fuel rods, F_t is the fission rate in the tramp uranium (fission s^{-1}) and F_f is the average fission rate per defective rod ($= FV$) (fission s^{-1}). For a typical CANDU-size fuel rod, assuming ~200 MeV fission^{-1}, $F_f = 1.489 \times 10^{13} \times P$, where P is the linear heat rating (in kW m^{-1}). The parameter H is a dimensionless factor to be applied for correction of the simple Booth diffusion model of Eq. (5) to account for precursor-diffusion effects. In fact, an enhanced diffusional release only results for those isotopes that have a relatively long-lived precursor (see Table 1), i.e., except for I-132 (where $H \approx 6$), this factor is the order of unity and can be ignored [26].

The model in Eq. (37) can be subsequently equated to a measured $(R/y)_{meas}$ ratio, as derived from steady-state coolant activity measurements via Eq. (35):

$$R_{meas} = (\lambda + \beta_p)N_c \Rightarrow \left(\frac{R}{y}\right)_{meas} = \left(\frac{\lambda + \beta_p}{\lambda}\right)\frac{A_c}{y}, \tag{38}$$

where $A_c = \lambda N_c$ is the measured coolant activity (in Bq) of a given isotope. Cumulative fission yields and decay constants for the iodine and noble gas isotopes are listed in Table 1. The cumulative fission yields y are dependent on the fuel burnup as a result of a changing fissile content of the naturally enriched UO_2 fuel as the ^{235}U is consumed and ^{239}Pu is produced:

$$y = \frac{(y_o w\sigma_f)_{U\text{-}235} + (y_o w\sigma_f)_{Pu\text{-}239}}{(w\sigma_f)_{U\text{-}235} + (w\sigma_f)_{Pu\text{-}239}}, \tag{39}$$

where y_o is the cumulative fission product yield for ^{235}U and ^{239}Pu in Table 1 from the Evaluated Nuclear Data File/Brookhaven (ENDF/B-V) [27], and σ_f is the microscopic thermal fission cross section (5.80×10^{-22} cm^2 for ^{235}U and 7.42×10^{-22} cm^2 for ^{239}Pu at 293.61 K). For

Table 1
Isotopic fission product data for iodine and noble gases

Isotope	Decay constant λ (s^{-1})	Fission product yield, y_o ($\times 10^{-2}$ atom/fission)[a]		Precursor correction factor, H
		^{235}U	^{239}Pu	
^{129}I	1.40×10^{-15}	0.744	1.49	1.0
^{131}I	9.98×10^{-7}	2.88	3.85	1.0
^{132}I	8.37×10^{-5}	4.30	5.39	6.0
^{133}I	9.26×10^{-6}	6.70	6.93	1.0
^{134}I	2.20×10^{-4}	7.71	7.27	1.4
^{135}I	2.91×10^{-5}	6.30	6.45	1.0
^{85m}Kr	4.30×10^{-5}	1.30	0.566	1.3
^{87}Kr	1.52×10^{-4}	2.52	0.987	1.3
^{88}Kr	6.78×10^{-5}	3.55	1.32	1.0
^{133}Xe	1.53×10^{-6}	6.70	6.98	1.1
^{133m}Xe	3.66×10^{-6}	0.190	0.233	1.2
^{135}Xe	2.12×10^{-5}	6.54	7.60	~1[b]
^{138}Xe	8.18×10^{-4}	6.42	5.12	1.0
^{137}Cs	7.29×10^{-10}	6.22	6.69	1.0

[a] Taken from Ref. [27].

[b] In the R/y analysis for this isotope, one normally applies an H factor which is dependent on the neutron flux φ and uses an effective decay constant $\lambda + \sigma_a\varphi$ where σ_a is the microscopic absorption cross section for ^{135}Xe. However, as a reasonable approximation, one can plot the R/y data point versus λ and apply an $H \sim 1$.

naturally enriched fuel, the initial ^{235}U specific fissile content is 7.116 g/kg U. The specific fissile content w (in g/kg U) is dependent on the fuel burnup B (in MW h/kg U), as shown in the following correlation based on reactor physics code calculations [26,28]:

$$w = 10^{(0.85095-0.0027604B)}, \quad \text{for } ^{235}\text{U} \tag{40a}$$

and

$$w = 4.20353 \times 10^{-3} + 4.0752 \times 10^{-2}B - 2.9702 \times 10^{-4}B^2 + 1.3035 \times 10^{-6}B^3 - 3.18147 \times 10^{-9}B^4 + 3.22097 \times 10^{-12}B^5, \quad \text{for } ^{239}\text{Pu}. \tag{40b}$$

Thus, a fitting of the model in Eq. (37) to at least three measured activities of the short-lived iodine species yields the model fitting parameters of v, A and c. To evaluate D' explicitly from the fitted value of A requires a knowledge of the number of failures (x) and the average power of the defective rods (i.e., in order to evaluate F_f).

A typical fitting of the model is shown in Fig. 2, where the different sources of release can be separated [29,30]. On a logarithmic plot if the R/y curve is independent of the decay constant, then the source of release is derived solely from uranium contamination. If there exists a linear relationship (with a slope lying between -0.5 and -1.5) then fuel failures are present. This latter dependence follows from Eq. (26) where if there is a large-sized failure with little holdup in the fuel-to-clad gap, i.e., $v \gg \lambda$, and a $\lambda^{-1/2}$ dependence results. On the other hand, for a small failure where $v \ll \lambda$, a $\lambda^{-3/2}$ dependence results. Fig. 2 shows a situation where in fact both fuel failures and uranium contamination are present so that a composite curve results.

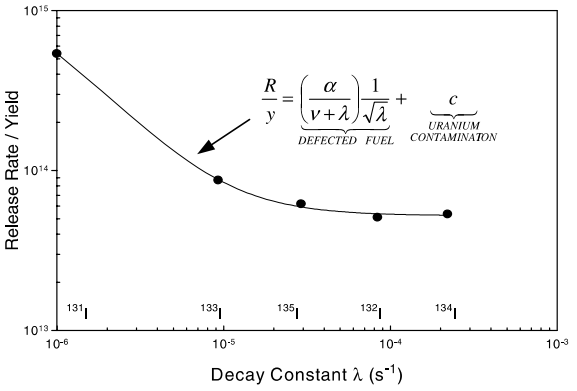

Fig. 2. Release versus decay constant plot for iodine. Data for the Douglas Point NGS, March 1982 (courtesy of Ontario Hydro). The defected fuel operated at an average linear heat rating of about 40 kW/m with an average burnup of 110 MW h (kg U)$^{-1}$. For the given fitting of the model in Eq. (37), $\alpha = vA = 1.155 \times 10^6$, $v = 1.378 \times 10^{-6}$ and $c = 5.220 \times 10^{13}$. The ^{132}I data point has been corrected for precursor effects by dividing it by H.

A precise scaling factor analysis requires that the independent model parameters D', v and c are known. Both the average fission rate of the defective rods, F_f, and the number of fuel failures, x, must be known a priori so that a specific determination of D' can be obtained from the fitted parameter A. If such information is unavailable, then D' (in s^{-1}) can be estimated from the experimentally derived correlations (for CANDU fuel) [26]:

$$D'_{\text{Iodine}} = 10^{9.857\log P - 25.1314}, \tag{41a}$$

$$D'_{\text{Noble Gas}} = 10^{8.632\log P - 23.4091} \tag{41b}$$

by assuming the average-core linear heat rating P (in kW/m). The quantity xF_f can be ascertained in a reverse fashion from an independent noble gas analysis using the fitted value of A for the measured noble gas coolant activities and the estimated value of D' from Eq. (41b).

In summary, the current steady-state treatment for the short-lived iodine species provides for a characterization of the defective fuel rods(s) and the amount of uranium contamination. This information is contained in the fitted escape rate coefficient v and average empirical diffusivity D' (relevant for x defective fuel rods operating at an average fission rate per defective rod of F_f). The amount of uranium contamination is contained in the parameter c which implicitly distinguishes the fission rate in the tramp uranium from that in the defective fuel rod(s). These parameters can then be employed in a scaling model to predict the coolant activity of the long-lived ^{129}I as detailed in Section 3.2.

3.2. I-129 coolant activity behaviour

In contrast to the short-lived isotopes, the long-lived ones do not necessarily reach an equilibrium in the reactor coolant. Consequently, the mass balance equation in Eq. (35), for the fission product inventory in the coolant, must be directly integrated (i.e., where $\lambda \sim 0$). Here the source release into the coolant from x defective fuel rods and uranium contamination is described by Eqs. (28), (32) and (36):

$$R_c^t(t) = xF_f y\left[(1 - e^{-vt}) + \frac{6v}{\pi^2}\sum_{n=1}^{\infty}\frac{e^{-n^2\pi^2D't} - e^{-vt}}{n^2(n^2\pi^2D' - v)}\right] + cy, \tag{42a}$$

where $c = F_t/2$. Eqs. (35) and (42a) can be numerically solved using a Runge-Kutta technique for a time-variable purification constant [29]. For short times, i.e., $\tau = D't \leqslant 0.1$, Eq. (42a) does not converge very quickly

and can be alternatively replaced by the short-time approximation

$$R_c^t(t) = x3F_f y\left[\frac{(1-e^{-\psi\tau})}{\psi} - \frac{\operatorname{erf}\sqrt{-\psi\tau}}{\sqrt{-\psi}}e^{-\psi\tau} - \tau + 2\sqrt{\frac{\tau}{\pi}}\right] + cy. \tag{42b}$$

Using Eq. (42a), the mass balance equation can be directly integrated, where assuming $A_c(0) = 0$, and a time-averaged coolant purification constant β_p,

$$\bar{\beta}_p = \frac{\int_0^t \beta_p(t')\,dt'}{t},$$

the coolant activity is given by:

$$\begin{aligned} A_c(t) = \mu x F_f y\Bigg\{ & \frac{1-e^{-\phi\tau}}{\phi} + \left(\frac{e^{-\psi\tau}-e^{-\phi\tau}}{(\psi-\phi)}\right) \\ & \times \frac{3}{\psi}\left[1-\sqrt{\psi}\cot\sqrt{\psi}\right] \\ & + 6\psi\sum_{n=1}^{\infty}\left(\frac{e^{-\phi\tau}-e^{-n^2\pi^2\tau}}{n^2\pi^2(n^2\pi^2-\psi)(n^2\pi^2-\phi)}\right)\Bigg\} \\ & + \lambda c y\left(\frac{1-e^{-\phi\tau}}{\bar{\beta}_p}\right), \end{aligned} \tag{43}$$

where $\mu = \lambda/D'$, $\psi = v/D'$ and $\phi = \bar{\beta}_p/D'$.

Thus, using the results of the short-lived analysis in Section 3.1, the resultant fitting parameters (v, D' and c) can be used in either Eqs. (35) (with $\lambda \sim 0$) and (42), or Eq. (43), to provide an estimate of the long-lived ^{129}I coolant activity as a function of time while the reactor is operating (i.e., prior to a reactor shutdown event). An expression for the coolant activity after reactor shutdown is detailed in Section 3.3.

3.3. Effect of reactor shutdown

When the reactor is shutdown, there is generally a greater burden of iodine activity in the PHT system due to the process of iodine spiking [31–34]. In this process, iodine deposited on internal fuel and clad surfaces surrounding the fuel-to-clad gap will be dissolved by liquid water following reactor shutdown and therefore free to migrate into the coolant. Hence, one must also consider this shutdown release.

The mechanism for iodine release from the gap is via ionic diffusion in liquid water, with possible convective assistance, which is generally quite rapid (i.e., within several hours), and hence it can be modelled as an instantaneous release process. Thus, for an impulsive source of release following shutdown, the rate of release of iodine into the coolant, $R_c^{S/D}$, can be described as an impulse function (or Dirac delta function) such that

$$R_c^{S/D}(t) = N_g\delta_+(t), \tag{44}$$

where N_g is the remaining stable iodine gap inventory at time t when the reactor is shutdown in accordance with Eq. (27), and δ_+ is the asymmetrical impulse function [35] with the property that

$$\int_0^t f(t')\delta_+(t')\,dt' = \begin{cases} 0, & \text{if } t \leqslant 0, \\ f(0), & \text{if } t > 0. \end{cases} \tag{45}$$

Again, the mass balance equation for the fission product inventory in the coolant for the stable isotopes is:

$$\frac{dN_c}{dt} = R_c^{S/D} - \beta_p N_c. \tag{46}$$

Thus, substituting Eq. (44) into (46), and integrating with the property of Eq. (45), yields:

$$N_c(t) = [N_{co} + N_g]e^{-\beta_p t} \Rightarrow A_c(t) = [A_{co} + A_{go}]e^{-\beta_p t}, \tag{47}$$

where $N_c(t)$ and $A_c(t)$ are the (long-lived) coolant inventory and activity at time t following a shutdown event, which is assumed to occur at $t = 0$, and N_{co} and A_{co} are the corresponding initial quantities at the time of shutdown. These latter quantities can be evaluated numerically from Eqs. (35) and (42), or from the analytic expression of Eq. (43). The quantity A_{go} is the initial gap activity when the reactor is shutdown which can be determined with Eq. (27), such that:

$$A_{go} = \left[\frac{(1-e^{-\psi\tau})}{\psi} - 6\sum_{n=1}^{\infty}\frac{e^{-\psi\tau}-e^{-n^2\pi^2\tau}}{n^2\pi^2(n^2\pi^2-\psi)}\right]\mu x F_f y. \tag{48}$$

The steady-state quantities A_{co} and A_{go} for short-lived species can be further determined. Rearranging Eqs. (37) and (38), the steady-state coolant activity is

$$A_{co} = \left[\left(\frac{v}{\lambda+v}\right)3\sqrt{\frac{D'}{\lambda}}\left(\frac{\lambda}{\lambda+\beta_p}\right)\right]xF_f y + c\left(\frac{\lambda}{\lambda+\beta_p}\right)y. \tag{49}$$

Similarly, using Eqs. (24) and (26), the available gap activity on shutdown is

$$A_{go} = \left[\left(\frac{\lambda}{\lambda+v}\right)3\sqrt{\frac{D'}{\lambda}}\right]xF_f y. \tag{50}$$

Eqs. (48) and (50), however, will slightly under-predict the iodine release on shutdown since they do not take into account iodine release from newly exposed fuel surfaces that result from fuel cracking during the shutdown event [33].

4. Discussion

Based on the steady-state analysis in Fig. 2, a coolant activity can be estimated for ^{129}I in the Douglas Point reactor. As discussed in Refs. [8,26], ~18 defective fuel rods operated in the Douglas Point reactor at a linear

heat rating of about 40 kW/m to an average fuel burnup of 110 MW h/kg U. The steady-state analysis yields the model fitting parameters of: $D' = 6.8 \times 10^{-10}$ s^{-1}, $v = 1.4 \times 10^{-6}$ s^{-1} and $c = 5.2 \times 10^{13}$ fission s^{-1}. The fuel residence time, t, can be estimated from the average burnup and linear power, considering that the Douglas Point fuel rod was manufactured with 0.710 kg U of heavy element and had a fuel length of 0.477 m. Thus, $t = 110$ MW h/kg U $\times$ 0.710 kg U/(40 kW/m $\times$ 0.477 m $\times 10^{-3}$ MW/kW $\times$ 24 h/d) $\sim$ 170 d. In addition, the data in Table 1 can be used where $\lambda = 1.40 \times 10^{-15}$ s^{-1} and $y = 1.08 \times 10^{-2}$ atom fission^{-1}. A heat rating of $P = 40$ kW m^{-1} will produce an average fission rate of $F_f = 5.96 \times 10^{14}$ fission s^{-1} per rod in the $x = 18$ defective rods. Further, assuming a purification flow rate through the I–X columns of 8.65 L s^{-1}, a column efficiency of 99%, and a PHTS volume of 67 000 L, a constant purification rate parameter of $\beta_p = 1.28 \times 10^{-4}$ s^{-1} is assumed in the analysis [28].

These various parameters in Eq. (43) yield the predicted coolant activity as shown in Fig. 3. Similarly, the coolant activity can be evaluated via a Runge-Kutta numerical integration of Eqs. (35) and (42a) using a time step of $h = 6$ h. In addition, the short-time approximation for the release rate in Eq. (42b) can be alternatively used (i.e., for $\tau = 0.010 \leqslant 0.1$). All three approaches typically deviate by less than $\sim$1%. As expected, the coolant activity after $\sim$170 d for ^{129}I, i.e., 390 Bq, is many orders of magnitude smaller than that observed for ^{131}I, where from Fig. 2 and Eq. (38), the ^{131}I activity is 1.3×10^{11} Bq. This result is in fact consistent with that seen in PWRs (see Section 4.1). As further shown in Fig. 3, most of the coolant activity in this particular case is derived from defective fuel operation with a smaller contribution resulting from the tramp uranium. The tramp uranium activity reaches an equilibrium in the coolant quite quickly for the given purification constant of $\beta_p = 1.28 \times 10^{-4}$ s^{-1} (i.e., this value corresponds to a short half-life of only 1.5 h for coolant cleanup with ion exchange).

As discussed in Section 3.3, any iodine remaining in the gap from the previous constant period of operation, will be rapidly released with water entry into the fuel-to-clad gap on reactor shutdown. This release will result in an additional burden of iodine activity in the coolant. Thus, if a shutdown were to occur after $\sim$170 d of operation (as for the given example), the initial coolant activity for ^{129}I at the start of the shutdown would be $A_{co} \sim 387$ Bq as seen in Fig. 3. The amount of iodine that would be quickly released from the gap is evaluated from Eq. (48) for $t = 170$ d as $A_{go} \sim 34\,770$ Bq. This 'iodine spike' release is several orders of magnitude greater than that determined while the reactor is operating. A similar 'iodine-spiking' phenomenon will also occur for the shorter-lived ^{131}I in accordance with Eqs. (47), (49) and (50) [31]. As described by Eq. (47), this combined activity

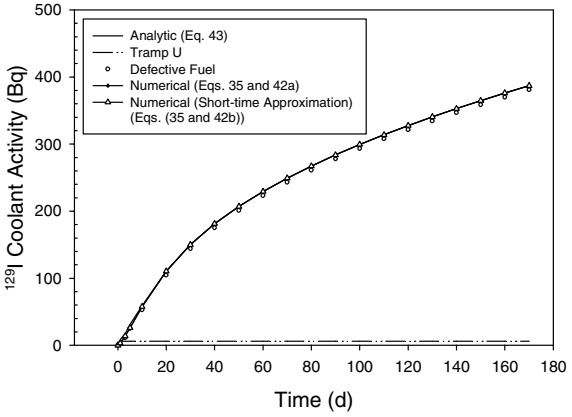

Fig. 3. Calculation of the coolant activity for ^{129}I as a function of time based on an analytical solution and using a numerical treatment.

will decay exponentially due to coolant purification with a half-life for the given case of 1.5 h.

4.1. Comparison to other measured and predicted ^{129}I coolant activities

As depicted in Table 2(panel A and B), routine data for both the radioiodines and other key radionuclides are available from CANDU power stations operated by Ontario Power Generation (Darlington Nuclear Generating Station (DNGS) and Pickering Nuclear Generating Station (PNGS)). In particular, a full complement of the short-lived iodine species are monitored. The ^{60}Co is the principal activation product.

On the other hand, the Electricité de France (EdF) have obtained actual measured coolant activity data for ^{129}I in several PWR plants (see Table 3) [36]. These activities can also be compared to those derived with a scaling from gamma measurements of ^{133}Xe and ^{137}Cs using the PROFIP code. Other measured coolant activities for ^{133}Xe, ^{131}I, ^{134}I and ^{137}Cs are also shown in Table 3. Indeed, the ratio of the measured PWR activities of ^{129}I/^{131}I, shown in Table 3, do indeed corroborate the previous analysis. For instance, a predicted ratio based on the measured short-lived ^{131}I data for the Douglas Point reactor, and the corresponding model estimation for the long-lived ^{129}I species, yield a comparable value of 390 Bq/1.3×10^{11} Bq $\sim 3 \times 10^{-9}$ to that observed in Table 3 (last column). This agreement provides further confidence in the model. However, it can also be seen in Table 3 that predictions of the long-lived ^{129}I activity, based on a given scaling, may vary by an order of magnitude or so from the corresponding measured value. It is worth pointing out that the measured ^{129}I/^{137}Cs ratio is essentially constant for several plants (i.e., within a factor of $\sim$50).

Table 2
Comparison between radioiodine and other key radionuclide PHTS concentrations

Radionuclide concentration (μCi/kg)	DNGS Unit 2 PHTS coolant		PNGS Units 1, 3-8 PHTS coolant	
	LM[a]	LD[b]	LM	LD
Panel A: DNGS and PNGS				
^{131}I	1.3	3.1	1.4	4.0
^{132}I	24.5	5.7	26.6	2.1
^{133}I	10.6	4.4	6.1	7.4
^{134}I	47.8	5.3	48.8	1.6
^{135}I	24.2	4.4	88.8	1.9
^{137}Cs	0.73	2.5	0.55	1.3
^{60}Co	0.30	2.3	1.96	2.9
Ratio of key radionuclides				
^{60}Co/^{137}Cs	0.41	1.9	1.8	–
^{60}Co/^{134}I	6.30E−03	4.0	–	–
^{132}I/^{131}I	19.0	2.7	12.6	2.4
^{133}I/^{131}I	8.2	2.1	4.6	3.7
^{134}I/^{131}I	37.1	2.7	22.9	1.9
^{135}I/^{131}I	18.8	2.2	2.3	2.1

	Unit 1		Unit 2		Unit 3		Unit 3	
	LM[a]	LD[b]	LM	LD	LM	LD	LM	LD
Panel B: DNGS								
^{60}Co	0.11	2.1	0.15	2.3	0.12	2.2	0.096	2.2
^{137}Cs	0.12	2.2	0.22	3.2	0.16	2.4	0.12	3.1
^{131}I	0.16	2.0	0.48	4.4	0.18	3.0	0.23	2.6
^{133}I	0.96	3.6	4.5	9.6	1.3	5.7	2.1	4.3
^{134}I	6.6	3.8	18	16.3	5.9	10.8	9.4	7.7
Ratio of key radionuclides								
^{60}Co/^{137}Cs	0.86	2.1	0.67	2.0	0.79	2.0	0.79	2.4
^{60}Co/^{134}I	0.017	4.1	0.0082	10.0	0.02	8.0	0.011	7.6
^{133}I/^{131}I	7.1	1.9	9.3	2.9	7.2	2.6	9.1	2.3
^{134}I/^{131}I	41	3.1	37	4.7	34	4.7	41	4.2

[a] LM = Log mean.
[b] LD = Log deviation.

The Battelle Pacific Northwest Laboratories designed a mixed-bed test resin sampling program to simulate a scaled-down version of the purification demineralizer system for a nuclear power plant [4]. Test resin columns were installed at 10 PWR and seven boiling water reactors (BWRs). The columns were operated with scaled-down flow rates to simulate the cleanup of the reactor coolant. Radioanalytical techniques were used to measure the concentrations of ^{129}I, ^{99}Tc, ^{90}Sr, ^{238}Pu, ^{239}Pu, ^{240}Pu and ^{14}C. Thermal emission mass spectrometry was used for the measurement of ^{129}I. Also, gamma-emitting radionuclides were measured by gamma spectrometry. The available concentration measurements of ^{137}Cs, ^{131}I and ^{129}I, and their respective ratios, for various plant test resin columns are shown in Table 4 [4]. Once again, these ratios are comparable with those depicted in Table 3, and are further supportive of the current analysis for CANDU fuel.

From a waste characterization perspective, the ratio of ^{129}I/^{137}Cs is of greater interest because this ratio can be readily applied with gamma scanning ^{137}Cs data to estimate ^{129}I levels in waste packages. As a first step, however, one can test the model against actual radionuclide activities of other iodine and cesium isotopes as readily measured in the PHTS of CANDU reactors. For instance, as depicted in Table 2B for the Darlington Nuclear Generating Station (DNGS), one can benchmark the model against the measured data of ^{137}Cs, ^{131}I, ^{133}I and ^{135}I, and then use the model to subsequently predict the ratio of ^{129}I/^{137}Cs.

For this analysis, it can be assumed that the diffusivity of cesium is approximately equal to that of iodine,

Table 3
Calculated and measured ^{129}I primary activities and measured ^{129}I/^{131}I ratios[a]

Plant	Cycle	Primary activities (MBq/t)					Measured ^{129}I/^{137}Cs	Measured ^{129}I/^{131}I
		^{133}Xe	^{131}I	^{134}I	^{137}Cs	^{129}I		
						Calculated from	Measured	
						^{133}Xe	^{137}Cs	
GRA3	9	1500	75	2500	45	3.6×10^{-8}	1.4×10^{-6}	6.1×10^{-8}	1×10^{-9}	8×10^{-10}
GRA6	5	1500	70	3000	0.85	4.4×10^{-8}	3.6×10^{-8}	2.9×10^{-8}	3×10^{-8}	4×10^{-10}
CHB1	8	80 000	1000	5000	100	6.5×10^{-6}	3.1×10^{-6}	5.0×10^{-6}	5×10^{-8}	5×10^{-9}
CHB2	7	9000	50	700	45	7.2×10^{-7}	1.4×10^{-6}	4.0×10^{-7}	4×10^{-9}	8×10^{-9}
BLA3	9	7000	80	1300	8	5.1×10^{-7}	2.4×10^{-7}	3.0×10^{-7}	4×10^{-8}	4×10^{-9}
BLA4	9	50 000	600	4000	150	4.0×10^{-6}	4.7×10^{-6}	1.3×10^{-6}	9×10^{-9}	2×10^{-9}
BUG2	13	1000	100	4000	1	5.8×10^{-8}	3.1×10^{-8}	$< 1.5 \times 10^{-6}$	$< 2 \times 10^{-6}$	$< 2 \times 10^{-8}$
GRA2	12	4000	200	8000	80	1.2×10^{-7}	2.5×10^{-6}	3.2×10^{-7}	4×10^{-9}	2×10^{-9}

[a] Taken from Ref. [36].

i.e., $D'_{\text{Cesium}} \sim D_{\text{Iodine}}$ as observed in high-temperature annealing tests [37]. The coolant purification constant β_p in Eq. (35) will depend on the respective removal efficiency (ε_p) for these species via $\beta_p = f_p \varepsilon_p / M$ (see Section 3.1). Moreover, the removal efficiency for cesium is particularly dependent on the operational age of the resin, in which the retention capability is reduced with time due to exchange with other ions such as Li. For instance, in the Battelle study, the fresh resin samples prepared by Battelle had a comparable efficiency for cesium and iodine $(\varepsilon_p)_{\text{Cesium}} \sim 0.9(\varepsilon_p)_{\text{Iodine}}$; however, this relative efficiency is significantly reduced for the reactor coolant purification resins in PWRs where $(\varepsilon_p)_{\text{Cesium}} \sim 0.2(\varepsilon_p)_{\text{Iodine}}$ [4].

The coolant activity data for the short-lived isotopes of ^{131}I, ^{133}I and ^{134}I in Table 2(panel B) can be fitted to the model of Eqs. (37) and (38), and the coolant activity data for ^{137}Cs can be modeled using Eq. (43), the relevant radionuclide data in Table 1 and appropriate parametric model values. Previously, Fig. 2 corresponded to a significant defect excursion in the Douglas Point NGS. Recent bundle defect rates for CANDU fuel are typically less than 0.1%, and thus it can be assumed that only a single failure exists ($x = 1$) [7]. Also, under normal circumstances, there would be much less tramp uranium in the PHTS (i.e., ~a few grams), as compared to the ~0.6 to 1 kg of UO_2 for the Douglas Point NGS excursion of Fig. 2 [26].

Thus, a steady-state analysis can be performed for the average of the short-lived iodine data in Table 2(panel B) for the Darlington NGS, based on a coolant mass of 280 Mg and nominal purification rate constant of $\beta_p \sim 4 \times 10^{-5}$ s^{-1} (i.e., ~10 kg s^{-1}). The fitted gap escape rate coefficient ($v_I \sim 4.4 \times 10^{-8}$ s^{-1}) suggests that the failed rod has a tight defect and the fitted value of A further implies an empirical diffusion coefficient of $D' = 4.0 \times 10^{-10}$ s^{-1}, which is consistent with a fuel rod power of ~40 kW/m as per Eq. (41a). Unfortunately, it was not known when the defect had actually occurred in reactor. For instance, an element containing a small manufacturing defect will typically hydride within ~20 d while a fretting defect, which is caused by debris in the coolant, could occur at any time during its operation [7]. It is also not clear when the defect was identified as well as its post defect residence time (i.e., if it was prematurely discharged). As such, in the current analysis it can be assumed that the defective bundle was discharged at its nominal discharge burnup of ~180 MW h/kg U. At a power level of 40 kW/m, the fuel would have to reside in core for a time of $t \sim 200$ d in order to achieve this burnup. As expected, the fitted parameter $c \sim 1.8 \times 10^{12}$ fission s^{-1} for the tramp contribution is a factor of ~30 smaller than that observed in Fig. 2.

Finally, using the fitted model parameters, a ^{137}Cs concentration of 0.14 μCi/kg is predicted with Eq. (43) (i.e., in agreement with the measured values in

Table 4
Cesium and iodine isotopic data for US Plant test resin columns

Name	Type	Date	Concentration (μCi/g resin)			Ratio	
			^{137}Cs	^{131}I	^{129}I	^{129}I/^{137}Cs	^{129}I/^{131}I
Indian Point Unit 2[a]	PWR	2/13/90	0.378	53.9	0.697×10^{-7}	1.8×10^{-7}	1.3×10^{-9}
Indian Point Unit 3	PWR	1/21/90	6.93	6.86	2.95×10^{-7}	4.3×10^{-8}	4.3×10^{-8}
Ginna	PWR	8/19/90	0.901	42.4	4.85×10^{-7}	5.4×10^{-7}	1.1×10^{-8}
Braidwood Unit 1	PWR	11/29/90	0.245	30.3	9.52×10^{-8}	3.9×10^{-7}	3.1×10^{-9}
Beaver Valley	PWR	11/9/90	1.84	2.89	2.11×10^{-8}	1.1×10^{-8}	7.3×10^{-9}
Vermont Yankee	BWR	4/12/90	1.78	64.4	3.5×10^{-7}	2.0×10^{-7}	5.4×10^{-9}
WNP-2	BWR	3/21/90	4.72	144	9.83×10^{-7}	2.1×10^{-7}	6.8×10^{-9}

[a] Average of samples IP-2-1, IP-2-3, IP-2-4, IP-2-5.

Table 2(panel B)) if it is assumed that $D'_{\text{Cesium}} \sim D'_{\text{Iodine}}$, $v_{\text{Cesium}} \sim 3v_{\text{Iodine}}$ and $(\varepsilon_p)_{\text{Cesium}} \sim 0.1(\varepsilon_p)_{\text{Iodine}}$ (in accordance with the PWR experience [4].) Using the same chemical-specific parameters, and relevant isotopic data in Table 1, the model predicts the ratio of ^{129}I/^{137}Cs to be $(2.6 \times 10^{-9}$ μCi/kg)/(0.14 μCi/kg) $\sim 2 \times 10^{-8}$.

This predicted ^{129}I/^{137}Cs ratio is once again comparable to measured activity ratios of these radionuclides in the primary coolant of PWRs as shown in Tables 3 and 4 (second last columns). This result follows somewhat since the coolant-activity ratio is independent of the number of fuel failures, and is relatively insensitive to the fuel rod power, gap escape rate coefficient and coolant purification constant. The time dependence of the coolant activities for ^{137}Cs, ^{129}I and their ratio are also shown in Table 5 for the assumed values of the gap escape rate coefficient and purification constants (i.e., Case I). The sensitivity of the model to the values of these two parameters is further shown in Table 5, for the case when both species have identical chemical behaviour such that $v_{\text{Cesium}} = v_{\text{Iodine}}$ and $(\varepsilon_p)_{\text{Cesium}} = (\varepsilon_p)_{\text{Iodine}}$ (i.e., Case II).

Interestingly, in both cases, the ^{129}I/^{137}Cs ratios are relatively constant with time; these values are also consistent with the observed range of values in Tables 3 and 4 for PWR fuel. The isotopic ratio for these cases depends on the relative values for the purification efficiency (which depends on the resin operational lifetime) and gap escape rates for the two nuclides. Moreover, there is little or no difference between the isotopic ratios for the tramp uranium contribution and for the total activity (i.e., resulting from both tramp uranium and defective fuel) for each case. In fact, when the diffusivities, gap escape rate coefficients and purification constants for cesium and iodine are identical (so that $\psi_{\text{Cesium}} \sim \psi_{\text{Iodine}}$, $\phi_{\text{Cesium}} \sim \phi_{\text{Iodine}}$ and $(\beta_p)_{\text{Cesium}} \sim (\beta_p)_{\text{Iodine}}$), as in Case II, then Eq. (43) and Table 5 indicate that these ratios should simply be equal to the ratio of the fission product activities in the fuel rod (as predicted, for example, with the ORIGEN code) [38]. A similar statement also holds for the spike release. If the coolant activity is derived solely from tramp uranium then the coolant activity ratios will similarly scale with the fission yield and decay constant. In fact, the slight variation in the isotopic ratio with time in Case II is simply due to a changing yield with burnup in accordance with Eqs. (39) and (40).

The corresponding ^{129}I/^{137}Cs ratio for Case I due to the spiking of the iodine and cesium on shutdown, can be further evaluated with Eq. (48), as $\sim 6 \times 10^{-7}$. This latter ratio is larger by a factor of $\sim$30 than that obtained during constant power operation.

Hence, these results suggest that it may be possible to correlate the coolant activity ratios of isotopes of different species and varying half-lives with those long-lived ones existing in the waste resins.

4.2. Limitations of the model

The current theoretical analysis is specifically applicable to the case of an average fuel failure and becomes less accurate in the case that there are several defective fuel rods operating at different linear heat ratings. The analysis may be further complicated by a range of defect sizes due to various states of fuel rod deterioration as a result of the clad hydriding process, and a varying coolant cleanup history. Moreover, the current treatment is an approximation at best since it implicitly assumes a constant power generation in the derivation of the fission product transport equations. In reality, the rods may have experienced a variable reactor history during several cycles of reactor operation (i.e., at different power levels), with the possible occurrence of a number of reactor shutdowns. In addition, on reactor shutdown and subsequent startup, fuel cracking may also result, exposing new fuel surfaces to the free void space.

The model also assumes that both the short and long-lived iodine isotopes have the same diffusivity considering their same physiochemical behavior. However, the diffusion coefficient that is utilized in the analysis is an empirical one, which accounts for many combined effects of atomic migration, bubble nucleation and resolution, bubble migration and coalescence, channel formation on grain faces, tunnel interlinkage on grain

Table 5
Time dependence of the total and tramp activities in the coolant[a]

Time t (d)	Coolant activity (μCi/kg)				$^{129}I/^{137}Cs$ ratio	
	Cs-137		I-129		Tramp U	Total activity (defective fuel + Tramp U)
	Tramp U	Total (defective fuel + Tramp U)	Tramp U	Total (defective Fuel + Tramp U)		
Case I: $v_{Cesium} = 3v_{Iodine}$ *and* $(\varepsilon_p)_{Cesium} = 0.1(\varepsilon_{p)_{Iodine}}$						
10	0.00195	0.00390	4.91×10^{-11}	7.35×10^{-11}	2.5×10^{-8}	1.9×10^{-8}
20	0.00203	0.00866	5.15×10^{-11}	1.24×10^{-10}	2.5×10^{-8}	1.4×10^{-8}
40	0.00204	0.0214	5.56×10^{-11}	2.72×10^{-10}	2.7×10^{-8}	1.3×10^{-8}
60	0.00205	0.0361	5.90×10^{-11}	4.67×10^{-10}	2.9×10^{-8}	1.3×10^{-8}
80	0.00206	0.0513	6.18×10^{-11}	7.00×10^{-10}	3.0×10^{-8}	1.4×10^{-8}
100	0.00207	0.0665	6.42×10^{-11}	9.62×10^{-10}	3.1×10^{-8}	1.5×10^{-8}
120	0.00208	0.0813	6.64×10^{-11}	1.25×10^{-9}	3.2×10^{-8}	1.5×10^{-8}
140	0.00208	0.0955	6.84×10^{-11}	1.55×10^{-9}	3.3×10^{-8}	1.6×10^{-8}
160	0.00209	0.109	7.02×10^{-11}	1.88×10^{-9}	3.4×10^{-8}	1.7×10^{-8}
180	0.00210	0.122	7.19×10^{-11}	2.21×10^{-9}	3.4×10^{-8}	1.8×10^{-8}
200	0.00210	0.134	7.35×10^{-11}	2.56×10^{-9}	3.5×10^{-8}	1.9×10^{-8}
Case II: $v_{Cesium} = v_{Iodine}$ *and* $(\varepsilon_p)_{Cesium} = (\varepsilon_p)_{Iodine}$						
10	0.000202	0.000303	4.91×10^{-11}	7.35×10^{-11}	2.4×10^{-7}	2.4×10^{-7}
20	0.000203	0.000489	5.15×10^{-11}	1.24×10^{-10}	2.5×10^{-7}	2.5×10^{-7}
40	0.000204	0.000999	5.56×10^{-11}	2.72×10^{-10}	2.7×10^{-7}	2.7×10^{-7}
60	0.000205	0.00163	5.90×10^{-11}	4.67×10^{-10}	2.9×10^{-7}	2.9×10^{-7}
80	0.000206	0.00234	6.18×10^{-11}	7.00×10^{-10}	3.0×10^{-7}	3.0×10^{-7}
100	0.000207	0.00310	6.42×10^{-11}	9.62×10^{-10}	3.1×10^{-7}	3.1×10^{-7}
120	0.000208	0.00391	6.64×10^{-11}	1.25×10^{-9}	3.2×10^{-7}	3.2×10^{-7}
140	0.000208	0.00474	6.84×10^{-11}	1.55×10^{-9}	3.3×10^{-7}	3.3×10^{-7}
160	0.000209	0.00559	7.02×10^{-11}	1.88×10^{-9}	3.4×10^{-7}	3.4×10^{-7}
180	0.000210	0.00646	7.19×10^{-11}	2.21×10^{-9}	3.4×10^{-7}	3.4×10^{-7}
200	0.000210	0.00733	7.35×10^{-11}	2.56×10^{-9}	3.5×10^{-7}	3.5×10^{-7}

[a] For both of these cases, $v_I = 4.4 \times 10^{-8}$ s^{-1} and $\beta_I = 3.83 \times 10^{-5}$ s^{-1} (as detailed in the text).

edges, microcracking and physical trapping [39]. Considering that the long-lived isotopes have a much greater half-life for survival (and hence a greater path length in the fuel pellet), these various processes may affect these isotopes differently. For instance, a slightly different diffusion coefficient has been proposed for the short- versus long-lived noble gas isotopes based on the application of the simple Booth diffusion representation to the analysis of sweep gas experiments at Halden [40,41].

5. Conclusions

1. A model has been developed to estimate the long-lived ^{129}I coolant activity as a function time during constant reactor operation. The model accounts for fission product release from both defective fuel rods and uranium contamination that may be present on in-core reactor surfaces. The current model is derived from a consideration of the physical release mechanisms. In particular, it is shown that diffusion is the dominant process for release from the fuel matrix to the fuel-to-clad gap in defective fuel at typical CANDU fuel power ratings. Low-temperature surface fission processes of recoil and knockout do not contribute significantly to the gap inventory. The subsequent release of volatile products from the gap to the primary coolant has been modelled as a first-order rate process. In comparison, due to lower temperatures that arise from fission heating in fuel debris, only direct recoil is an important mechanism of release into the primary coolant from uranium contamination deposited on in-core surfaces. Thus, the resulting activity in the primary heat transport system can be evaluated from a mass balance, considering these various sources, and a loss due to coolant cleanup operations.

A model has been further developed to predict the ^{129}I activity spike that occurs following reactor shutdown from the release of the available gap inventory (stored as a water-soluble deposit) in the defective fuel rods. This additional activity results in a further iodine burden in the PHTS.

2. A coolant activity analysis of the short-lived iodine species can be used to provide the relevant transport parameters needed for the long-lived ^{129}I predictive

model (because both the short and long-lived iodine species have the same physiochemical properties). Based on a steady-state analysis, this approach yields the empirical diffusion coefficient and gap escape rate coefficient for defective fuel, and the tramp uranium fission rate. A calculation was performed for the Douglas Point NGS, in which there were ~18 defective fuel rods operating at ~40 kW/m, with a corresponding fuel loss of about ~0.6 to 1 kg of UO_2 in the primary heat transport system. The resulting ratio between the measured ^{131}I coolant activity and the ^{129}I prediction after ~170 d of reactor operation with defective fuel was 3×10^{-9}. This value is in good agreement with observed coolant activity ratios for $^{129}I/^{131}I$ in French PWRs (i.e., 4×10^{-10} to 8×10^{-9}), and for US BWRs and PWRs (i.e., 1×10^{-9} to 4×10^{-8}) obtained from test resin column samples in a study by the Battelle Pacific Northwest Laboratories. Moreover, model parameters can be derived for cesium, by matching the model predictions to measured coolant activity concentrations of ^{137}Cs and short-lived radioiodines. In fact, using these speciation-specific parameters in the current model, a predicted coolant activity ratio for $^{129}I/^{137}Cs$ of $\sim 3 \times 10^{-8}$ was obtained for the Darlington NGS. Once again, this value is in good agreement with that observed in French and US PWRs for the given isotopic ratio.

For the Douglas Point NGS analysis, with reactor shutdown, the stored gap inventory that is released from the fuel rod results in a ~100-fold iodine spike in the coolant activity level.

3. The application of the current model in Eq. (43) suggests that when cesium and iodine have identical parameter values, the ratio between ^{129}I and ^{137}Cs can be calculated directly from radionuclide inventories in used fuel.

Acknowledgements

The current project was identified and managed by Kinectrics Inc., and financially supported by Ontario Power Generation. The authors would also like to acknowledge partial support from the Director General Nuclear Safety in the preparation of this paper.

References

[1] A. Husain, International Workshop on Determination and Declaration of Nuclide Specific Activity Inventories in Radioactive Wastes, Cologne, Germany, 2001.
[2] A. Lemmens, Radwaste Characterization, Belgatom Seminar, Brussels, Belgium, 17 October 2000.
[3] C. Leuthrot, Calculation of the Activity of Fission Products and Actinides in the Primary Systems of Pressurized Water Reactors, PROFIP Code Version IV, Commissariat à l'Energie Atomique, Technical Report DEC/SECA/LCC/95-243, 1995.
[4] Vance and Associates, RADSOURCE, Volume 1, Part 1: A Scaling Factor Prediction Computer Technical Manual and Code Validation, Electric Power Research Institute report, EPRI TR-101969, December 1992.
[5] J. Vance, Topical Report for 3R-STAT: A Tc-99 and I-129 Release Analysis Computer Code, United States Nuclear Regulatory Commission, September 1994.
[6] B.J. Lewis, J. Nucl. Mater. 160 (1988) 201.
[7] B.J. Lewis, R.D. MacDonald, N.V. Ivanoff, F.C. Iglesias, Nucl. Technol. 103 (1993) 220.
[8] B.J. Lewis, J. Nucl. Mater. 148 (1987) 28.
[9] G.V. Kidson, J. Nucl. Mater. 88 (1980) 299.
[10] B.J. Lewis, C.R. Phillips, M.J. Notley, Nucl. Technol. 73 (1986) 72.
[11] S.D. Beck, The Diffusion of Radioactive Fission Products From Porous Fuel Elements, USAEC Report BMI – 1433, April 1960.
[12] Background and Derivation of ANS 5.4 Standard Fission Product Release Model, NUREG/CR-2507, US Nuclear Regulatory Commission, January 1982.
[13] A.H. Booth, AECL-700, Atomic Energy of Canada Limited, 1957.
[14] J.F. Ziegler, J.P. Biersack, SRIM: The Stopping and Range of Ions in Matter, SRIM-2000 (v. 4), IBM-Research, Yorktown, New York, 1999.
[15] D.R. Olander, Fundamental Aspects of Nuclear Reactor Fuel Elements, TID-26711-P1, 1976, p. 289.
[16] G. Nilsson, J. Nucl. Mater. 20 (1966) 215.
[17] M.D. Rogers, J. Nucl. Mater. 22 (1967) 103.
[18] R.M. Carroll, O. Sisman, Nucl. Sci. Eng. 21 (1965) 147.
[19] R. Beraha, G. Beuken, G. Frejaville, C. Leuthrot, Y. Musante, Nucl. Technol. 49 (1980) 426.
[20] D.L. Burman, O.A. Correal, H.W. Wilson, H. Kunishi, L.H. Boman, in: Proc. Int. Top. Mtg. LWR Fuel Performance, Avignon, France, American Nuclear Society, 21–24 April 1991, p. 363.
[21] C.E. Beyer, Methodology Estimating Number of Failed Fuel Rods and Defect Size, EPRI NP-6554, Electric Power Research Institute, September 1989.
[22] M. Pourbaix, Atlas of Electrochemical Equilibria in Aqueous Solutions, Pergamon, New York, 1966, p. 209.
[23] C. Wise, J. Nucl. Mater. 136 (1985) 30.
[24] B.J. Lewis, B. Andre, B. Morel, P. Dehaudt, D. Maro, P.L. Purdy, D.S. Cox, F.C. Iglesias, M.F. Osborne, R.A. Lorenz, J. Nucl. Mater. 227 (1995) 83.
[25] G.M. Allison, R.F.J. Robertson, Atomic Energy of Canada Limited report AECL-1338, September 1961.
[26] B.J. Lewis, R.J. Green, C.W.T. Che, Nucl. Technol. 98 (1992) 307.
[27] S.L. Jurgilas, Direct and Cumulative Fission Product Yields Based on ENDF/B-V, CRNL-2478, Chalk River Laboratories, unpublished report, February 1983.
[28] R.J. Green, A Prototype Expert System for Fuel Failure Monitoring in CANDU Power Reactors, MEng thesis, Royal Military College of Canada, April 1990.
[29] W.H. Press, S.A. Teukolsky, W.T. Vetterling, B.P. Flannery, Numerical Recipes in C, The Art of Scientific Computing, 2nd Ed., Cambridge University, New York, 1996.
[30] SigmaPlot, Version 4.01, SPSS, 1986–1997.

[31] B.J. Lewis, D.B. Duncan, C.R. Phillips, Nucl. Technol. 77 (1987) 303.
[32] W.N. Bishop, Iodine Spiking, EPRI NP-4595, Electric Power Research Institute, 1986.
[33] B.J. Lewis, R.D. MacDonald, H.W. Bonin, Nucl. Technol. 92 (1990) 315.
[34] B.J. Lewis, F.C. Iglesias, A.K. Postma, D.A. Steininger, J. Nucl. Mater. 244 (1997) 153.
[35] G.A. Korn, T.M. Korn, Mathematical Handbook for Scientists and Engineers, second Ed., McGraw-Hill, New York, 1968, p. 879.
[36] C. Leuthrot, P. Ridoux, A. Harrer, Scaling Factors for ^{129}I in PWR's Wastes, unpublished.
[37] B.J. Lewis, B. Andre, G. Ducros, D. Maro, Nucl. Technol. 116 (1996) 34.
[38] A.G. Croft, Nucl. Technol. 62 (1983) 335.
[39] F.C. Iglesias, B.J. Lewis, P.J. Reid, P. Elder, J. Nucl. Mater. 270 (1999) 21.
[40] J.A. Turnbull, E. Kolstad, in: Seminar of Fission Gas Behaviour in Water Reactor Fuels, 26–29 September 2000, Cadarache, France.
[41] R.J. White, J. Nucl. Mater. 295 (2001) 133.